



Modeling and Integral Sliding Mode Control of a Roll-yaw Seeker by Removing the Singularity Condition

Mahsa Ghasemi¹, Hadi Nobahari², Hamed Mohammadkarimi¹ *

¹ Department of Aerospace Engineering, Amirkabir University of Technology, Tehran, Iran.

² Department of Aerospace Engineering, Sharif University of Technology, Tehran, Iran.

ABSTRACT: This paper aims to model and sliding mode control of a roll-yaw seeker. In the roll-yaw seeker, a singularity occurs when the seeker is directed precisely to a target, and the seeker will lose the target. Thus, the Controller design should contain a tracking strategy to deal with the singularity. In this paper, Newton-Euler's method is applied to the dynamic model of a roll-yaw seeker's roll and yaw gimbals. The dynamics of the roll-yaw seeker are highly nonlinear. Also, unmodeled uncertainties and perturbations reduce the model's reliability. A two-input, two-output integral sliding mode controller is designed to control the nonlinear dynamics of the seeker and deal with uncertainties. The numerical simulation results show that all three stabilization, tracking, and guidance loops in both roll and yaw channels have acceptable performance. Also, it is shown that the controller has good robustness.

Review History:

Received: Sep. 08, 2024

Revised: Feb. 15, 2025

Accepted: Feb. 16, 2025

Available Online: Feb. 19, 2025

Keywords:

Roll-yaw Seeker

Sliding Mode Control

Stabilization

Tracking

Guidance

1- Introduction

In some air-to-air flying vehicles, an optical seeker detects and tracks the target and moves toward it. After positioning the seeker towards the target, the control commands of the servos are calculated and applied based on the tracking error. With the development of optics and electronics, the optic seeker is used in many flying vehicles, especially air-to-air ones.

Gimbaled seekers are structurally divided into three-axis and two-axis seekers. A three-axis seeker is used where a wide field of regard is required. This type of seeker needs a large installation space, so it has been used in large-diameter flying vehicles, while the two-axis seeker requires less space to be installed and used in smaller-diameter vehicles. However, due to the rotational limitation, the two-axis seeker provides less field of regard than the three-axis type. Two-axis seekers are divided into "pitch-yaw" and "roll-pitch" seekers.

The conventional type in most flying vehicles is the pitch-yaw seeker [1]. Two independent control channels control this type of seeker (pitch and yaw), which have less coupling and easier control but have a limited field of regard. Therefore, high-maneuver targets get out of sight faster, and the target is missed. Instead, the roll-yaw seeker has a wide field of regard, demonstrating its superiority over the pitch-yaw seeker. The roll-yaw seeker structure consists of a roll gimbal

and a yaw gimbal mounted on the flying vehicle's body. The outer gimbal rolls relative to the body, and the inner gimbal yaws relative to the outer gimbal. Detectors and rate gyros are positioned on the inner gimbal.

To track and detect the target, the outer gimbal rolls, and then the inner gimbal yaws toward the target. Therefore, the outer gimbal dynamic should be faster than the inner gimbal. The dynamics of these two channels are coupled, and their equations of motion are highly nonlinear. In addition, there are uncertainties due to the connection of cables to each of the gimbals, modeling errors, frictional moments, and disturbances such as the target maneuver.

The outer gimbal rotates to 360 degrees, and the inner gimbal rotates to about 90 degrees, resulting in a wide field of regard. The seeker's goal is stabilizing the line of sight (LOS) rate in the inertial space, and this requires placing the x-axis of the seeker's inner frame toward the target. However, when the tracking error is about zero, the roll rate (outer gimbal angular rate) becomes infinite, and a singularity occurs. In other words, the Singularity occurs in the roll-yaw seeker when is directed to a target. The singularity, or the so-called "zenith-past problem," occurs when the yaw error becomes zero. As this angle becomes zero, the term $1/0$ appears in the roll frame kinematic equation, which ultimately causes the roll rate to become infinite. This issue is fully explained in the following sections. The singularity of the roll-yaw seeker is its disadvantage that must be eliminated. Figure 1 shows a

*Corresponding author's email: h.mohammadkarimi@aut.ac.ir



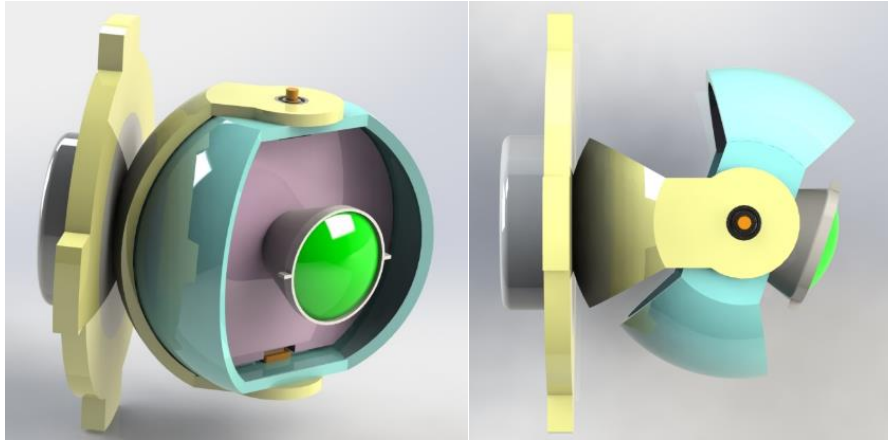


Fig. 1. Roll-yaw seeker

schematic of a roll-yaw seeker.

In most references discussed in the following, the outer gimbal rolls and the inner gimbal yaws are named a “roll-pitch” seeker. It should be noted that the singularity in the roll-yaw seeker is usually named the “zenith pass problem” in previous research. According to Authers’ knowledge, there needs to be more research on the LOS estimation of Roll-Pitch seekers.

In reference [2], the target tracking using a roll-pitch seeker is investigated. The tracking errors of angular frames (roll and pitch frames) are modeled according to the coordinates of the target in the detector, the geometry of the roll-pitch seeker, and the seeker’s position relative to the flying vehicle. This model is used to design the closed-loop controller for the roll-pitch seeker. In reference [3], a method is presented to solve the zenith pass problem in a roll-pitch seeker. In this paper, based on the relation between the seeker’s performances and the design parameters, the seeker’s work area is divided into three parts, and the control strategy of each section is formulated separately. The simulation results show this strategy prevents the zenith pass problem in seeker performance.

Reference [4] focuses on solving the roll-pitch seeker singularity problem. In this paper, to prevent the infinite roll rate, according to the roll and pitch angles, the LOS rate, and the derivation from the center of the image plane, the roll angle control strategy is divided into three areas with the minimum, medium, and maximum rotation rates. With this segmentation, the control is performed so that when the target appears in the area around the singularity point, it remains on the screen and does not miss. In the reference [5], according to Lee’s algebra theory, the kinematics of the roll-pitch seeker is investigated by the product of the exponential (POE) multiplication method, and the LOS stability equation of motion is written. Then, different schemes of configuration and gyroscope installation on the outer gimbal are represented, and the advantages and disadvantages of each configuration

are stated.

In the reference [6], four optimal control methods have been designed to minimize the roll angle, and the effectiveness of these algorithms has been shown. In reference [7], an optimal control method is used to control the roll-pitch seeker. This method’s cost function includes the seeker’s control energy vector and tracking error vector. When the target is far from the singularity point, the seeker’s outer gimbal must rotate fast to track the target. On the other hand, the sensitivity of the outer gimbal to the target position should be minimized near the areas around the singularity point. In this case, singularity does not occur. In the cost function, the weight functions of the control energy vector and the error vector are selected to accomplish the proposed control scenario.

In reference [8], an estimator is initially used to predict the area where the singularity occurs and to obtain the angular error between the gimbals frames and the LOS. The model parameters are updated using the least square method and with the information obtained from consecutive measurements. Then, a Predictive Functional Control is designed for the outer frame to reduce tracking error. Reference [9] examines a method for obtaining roll-pitch seeker data in anti-infrared decoy state conditions. Kalman filter is used to estimate the rotation rate of the LOS rate. The proposed method has been validated using numerical simulations in the presence of various maneuvers. Reference [10] uses a fuzzy PID controller considering gyros noise. The fuzzy PID controller is compared to a PI controller.

In reference [11], the usage of a roll-pitch seeker on a flying vehicle is investigated. This paper focused on the effect of a parasitical loop of a roll-pitch seeker on the dynamic stability of a spinning vehicle. The results indicate that the stability of the spinning vehicle is closely related to the disturbance rejection rate and rolling rate of the roll-pitch seeker and the design indices of autopilot. In reference [12], a roll-pitch seeker’s tensorial modeling and simulation are studied. The singularity problem of the roll-pitch seeker

needs to be investigated in these papers.

Reference [13] proposes a novel snake-hot-eye-assisted multi-process-fusion target tracking method for roll-pitch semi-strap-down infrared imaging seekers. The proposed method overcomes the drawbacks of traditional methods, such as the need for more calculation accuracy of the line-of-sight angular rate and the inability to measure the flying vehicle-target distance directly. The proposed method consists of two main parts: a snake-hot-eye visual bionic imaging guidance method and a multi-process-fusion integrated filter model of relative motion and angle tracking. The snake-hot-eye visual bionic imaging guidance method estimates the flying vehicle-target relative distance from the infrared images by imitating the snake-hot-eye visual mechanism. It improves the observability of the filter model. The multi-process-fusion integrated filter model of relative motion and angle tracking integrates the information from the snake-hot-eye visual bionic imaging guidance method and the inertial measurement unit (IMU) to track the target accurately.

Simulation results show that the proposed method can track the target accurately even in the presence of large maneuvering targets and high background noise. The proposed method has the potential to improve the performance of guidance systems.

Reference [14] investigates the influence of the roll-pitch seeker's parasitic loop on the guidance system's stability. The scale deviation between the detector causes the parasitic loop, the frame angle sensor, and the angular rate gyroscope. The authors first establish a mathematical model of the parasitic loop. Then, they analyze the stability of the guidance system with the parasitic loop using the Routh-Hurwitz criterion. The results show that the parasitic loop can significantly impact the guidance system's stability.

The positive feedback characteristics of the parasitic loop can lead to instability, while the negative feedback characteristics can improve stability. Using a feedback controller, the authors also propose a method to compensate for the parasitic loop. The simulation results show that the proposed method can effectively improve the stability of the guidance system. The paper's findings have important implications for designing and analyzing guidance systems for roll-pitch seekers.

Reference [15] introduces an Extended State Observer-based Disturbance Rejection Rate compensation method for the roll-pitch seeker. Roll-pitch seeker specifications and DRR limits are analyzed. Also, the effect of different perturbation torques has been investigated. The modeling and simulation of the guidance loop using a roll-pitch seeker are presented with the proposed compensation method and then compared with existing methods, such as the Kalman filter. The simulation results confirm the better results of the proposed method.

[16] introduced an ESO-based Disturbance Rejection Rate (DRR) compensation method for roll-pitch seekers. It analyzed seeker characteristics and defined DRR for its two frames, examining the method's influence on dimensionless miss distance. Results highlight the method's precision,

applicability, and adjustability, demonstrating its efficacy in reducing miss distance across various input error types.

Reference [17] explores how disturbance rejection rate (DRR) and parasitic loop parameters impact the stability of roll-pitch seeker guidance systems. It establishes DRR models for various disturbances and proposes an optimal model considering sensor scale deviations. By employing Lyapunov stability criteria, simplifies the guidance system model and identifies three stability conditions. Simulation results, including Nyquist plots, analyze the effects of DRR parameters on system stability, providing insights for related analyses.

[18] proposes a solution to the over-tracking problem of roll-pitch seekers, which hampers their engineering applications despite their wide field of view. By calculating the roll frame angle using the angular rate of the projectile line of sight when the pitch frame angle is small, the method effectively improves overhead tracking control, as shown in simulation results.

In reference [19] to simplify the tracking process of the roll-pitch seeker, By analyzing the working principle and characteristics of the roll-pitch seeker, a new method for tracking targets based on the resolution rotation mechanism is proposed which can applied in engineering practice. According to Dynamic experiments, the image rotation method is still applicable in the presence of carrier disturbances; compared with traditional coordinate conversion methods, the resolution rotation method significantly improves tracking accuracy.

[20] explores how disturbance rejection rate (DRR) affects the stable tracking of a maneuvering target with roll-pitch seekers. It analyzes the seeker's tracking principle, establishes a control scheme, and derives DRR transfer functions using different torque models. Simulations reveal that spring torque DRR greatly impacts tracking under low-frequency disturbances while damping torque DRR mainly affects tracking accuracy.

[21] investigates disturbance rejection rate (DRR) in roll-pitch seekers, impacting aircraft attitude and guidance accuracy. It analyzes seeker tracking principles, devises a control scheme, and finds that DRR significantly affects tracking angle and accuracy, especially spring torque DRR under low-frequency disturbances or maneuvering targets while damping torque DRR influences overall tracking accuracy.

Reference [22] tackles singularity challenges in terminal guidance using roll-pitch seekers near a projectile's longitudinal axis. It suggests a control strategy to mitigate zenith-pass singularity problems under an oblique scheme, ensuring stable target tracking while avoiding singularity areas by adjusting the projectile's roll motion based on the seeker's pitch frame angle. This approach, superior to adding a third axis, maintains seeker compactness and lightness. It also outperforms sub-region variable parameter control methods, resolving tracking failures during static and deceleration control, as evidenced by simulations showcasing high accuracy and system stability.

According to previous research, the integral sliding mode

control approach has yet to be used to control roll-pitch seekers. In this paper, after accurate modeling of the seeker dynamic, a new method is proposed to eliminate zenith-pass singularity. In the seeker under study, the outer gimbals rolls and the inner yaws. The name roll-yaw seeker is used to match the wording and physics of the seeker.

First, the accurate mathematical modeling of the seeker is derived. Then, the roll-yaw control for an air-to-air flying vehicle was designed so that it was resistant to disturbances and uncertainties. Given this seeker's nonlinear and coupled dynamics, as well as model uncertainties, a multi-input, multi-output integral sliding mode control approach is used. It is also suggested that when the seeker is directed to a target, singularity does not occur; according to the authors' knowledge, this control approach and singularity avoidance method have yet to be used in the control of the roll-yaw seeker.

The structure of the present paper is as follows: In section 2, after defining the coordinate systems in the present problem, the seeker kinematic equations of motion will be driven. Section 3 introduces the structure of the roll-yaw seeker control loops, including the stabilization and tracking loops. After that, the sliding mode control method is introduced, and it will be designed for the two roll and yaw channels of the stabilization loop. In section 4, the simulation results of the stabilization and tracking loop will be presented, and in section 5, a conclusion will be made.

2- The Roll-yaw Seeker Modeling

In this section, the mathematical modeling of the roll-yaw seeker is presented by introducing the frames and coordinate systems. Newton-Euler's method has been used to drive the dynamic model.

2- 1- Frames and coordinate systems definitions

To drive the kinematic and dynamic equations of motion for the seeker, inertial, body, outer, and inner frames are used. In this research, the flat-earth frame is considered as the inertial reference frame. The center of the flat-earth frame is located at an arbitrary point on the earth's surface, and its first axis is defined to the north, second to the east, and third is downward according to the right-hand rule. Body and inertial reference frames are linked using a transformation matrix. This matrix transfers the inertial reference frame to the body frame [23].

$$[T]^{BI} = \begin{bmatrix} \cos \theta \cos \psi & \cos \theta \sin \psi & -\sin \theta \\ \sin \phi \sin \theta \cos \psi & \sin \phi \sin \theta \sin \psi & \sin \phi \cos \theta \\ -\cos \phi \sin \psi & -\cos \phi \cos \psi & \\ \cos \phi \sin \theta \cos \psi & \cos \phi \sin \theta \sin \psi & \cos \phi \cos \theta \\ +\sin \phi \sin \psi & -\sin \phi \cos \psi & \end{bmatrix} \quad (1)$$

In the above equation, ϕ , θ and ψ represent the body frame's roll, pitch, and yaw angles concerning to the inertial frame, respectively. In Figure 2, the body frame, the inner and the outer frames are also shown. The coordinate center of all three frames is fixed and located on the center of mass of the flying vehicle. In this figure, X_B , Y_B and Z_B show the main axes of the body frame. The outer frame of the seeker (relative to the body frame) can move with one degree of freedom of roll. The body frame coincides with the outer frame by rotating as much as the angle ϕ_s around the axis X_B . X_R , Y_R and Z_R represent the main axes of the outer frame (roll frame). By rotating the outer frame by ψ_s angle around the axes Z_R , the inner frame (yaw frame) is obtained with axes X_Y , Y_Y and Z_Y . The inner frame is also called the line of sight frame. The transfer matrix from the body frame to the outer frame and the transfer matrix from the outer frame to the inner frame is calculated using the following equations.

$$[T]^{RB} = \begin{bmatrix} 1 & 0 & 0 \\ 0 & \cos \phi_s & \sin \phi_s \\ 0 & -\sin \phi_s & \cos \phi_s \end{bmatrix} \quad (2)$$

$$[T]^{YR} = \begin{bmatrix} \cos \psi_s & \sin \psi_s & 0 \\ -\sin \psi_s & \cos \psi_s & 0 \\ 0 & 0 & 1 \end{bmatrix} \quad (3)$$

When the target is not in line with the axis of the seeker detector (X_Y), to express the error angle between the inner frame's first axis and the target's line of sight, it is necessary to define two interior frames. The roll interior frame (denoted by the axes ΔX_R , ΔY_R and ΔZ_R) is obtained from the line-of-sight frame rotation around the X_Y axis of size $\Delta \phi_s$. The yaw interior frame is obtained from the rotation around the ΔZ_R axis of size $\Delta \psi_s$. This frame is shown in Figure 2 with the axes ΔX_Y , ΔY_Y and ΔZ_R . $\Delta \phi_s$ And $\Delta \psi_s$ are the roll error and the yaw error respectively required by the seeker X_Y axis to be positioned towards the target.

2- 2- Kinematic equations of motion

In order to derive the seeker's kinematic equations, the target position is expressed in the LOS coordinate system. According to the target's relative position, the two-degree-of-freedom seeker must rotate so that the sensor connected to the inner frame (the first axis of the inner frame) is directed to the target with two roll and yaw movements. Figure 3 shows the frames used in the roll-yaw seeker to express kinematic equations. By defining the position vector of the target relative to the flying vehicle, and from the following relations, $\Delta \phi_s$ and $\Delta \psi_s$ are obtained in which x_t , y_t and z_t are the components of this vector in the inner frame.

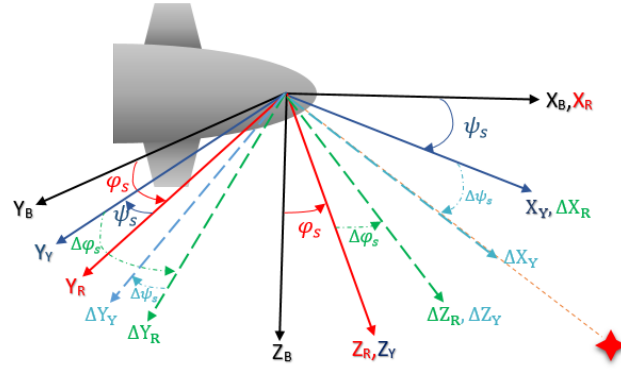


Fig. 2. Introducing frameworks used in Roll-Pitch seeker modeling

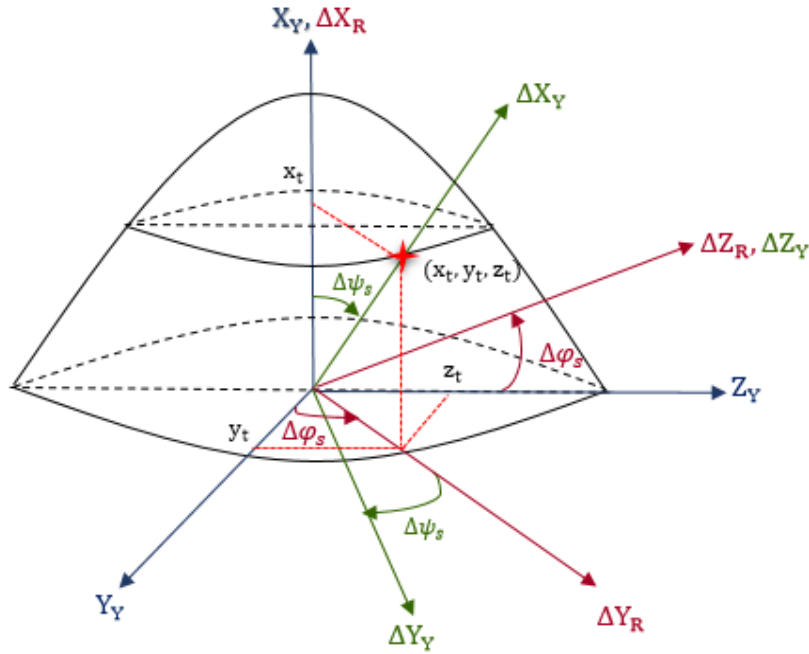


Fig. 3. The interior frames relative to the inner frame

$$\Delta\varphi_s = \tan^{-1}\left(\frac{z_t}{y_t}\right) \quad (4)$$

$$\Delta\psi_s = \tan^{-1}\left(\frac{\text{sgn}(y_t)\sqrt{z_t^2 + y_t^2}}{x_t}\right) \quad (5)$$

3- Dynamic equations of motion

In this section, the seeker's dynamic equations of motion are derived. Since the outer frame of the seeker rolls and the inner frame yaws, we first obtain the angular velocity of each frame. The angular velocity vector of the body frame WRT the inertial frame, and expressed in the body frame is:

$$[\omega^{BI}]^B = \begin{bmatrix} p \\ q \\ r \end{bmatrix} \quad (6)$$

In equation (6), the components p , q and r represent the roll, pitch and yaw rates of the flying vehicle, respectively. The angular velocity of the outer frame WRT the inertial frame, and expressed in the outer frame, and also the angular velocity of the inner frame WRT the inertial frame, and expressed in the inner frame, are also written as follows:

$$\begin{bmatrix} \omega^{RI} \end{bmatrix}^R = \begin{bmatrix} p_R \\ q_R \\ r_R \end{bmatrix} \quad (7)$$

$$\begin{bmatrix} \omega^{YI} \end{bmatrix}^Y = \begin{bmatrix} p_Y \\ q_Y \\ r_Y \end{bmatrix} \quad (8)$$

Considering ω^{YB} as follows:

$$\omega^{YB} = \omega^{YR} + \omega^{RB} \quad (9)$$

By the tensor expression of the equation (9) in the inner frame, (10) is obtained as follows:

$$\begin{bmatrix} \omega^{YB} \end{bmatrix}^Y = \begin{bmatrix} \omega^{YR} \end{bmatrix}^Y + \begin{bmatrix} \omega^{RB} \end{bmatrix}^Y = \begin{bmatrix} 0 \\ 0 \\ \dot{\psi}_s \end{bmatrix} + [T]^{YR} \begin{bmatrix} \dot{\phi}_s \\ 0 \\ 0 \end{bmatrix} \quad (10)$$

where $[T]^{YR}$ is the transformation matrix from the outer frame to the inner frame, $\dot{\psi}_s$ is the rotation rate of the inner frame relative to the outer frame, and $\dot{\phi}_s$ is the rotation rate of the outer frame relative to the body frame. Having $[\omega^{BI}]^Y$ and $[\omega^{YB}]^Y$, $[\omega^{YI}]^Y$ is obtained as follows:

$$\begin{bmatrix} \omega^{YI} \end{bmatrix}^Y = \begin{bmatrix} \omega^{YB} \end{bmatrix}^Y + \begin{bmatrix} \omega^{BI} \end{bmatrix}^Y \quad (11)$$

$$\begin{bmatrix} p_Y \\ q_Y \\ r_Y \end{bmatrix} = \begin{bmatrix} 0 \\ 0 \\ \dot{\psi}_s \end{bmatrix} + \begin{bmatrix} \cos \psi_s & \sin \psi_s & 0 \\ -\sin \psi_s & \cos \psi_s & 0 \\ 0 & 0 & 1 \end{bmatrix} \begin{bmatrix} \dot{\phi}_s \\ 0 \\ 0 \end{bmatrix} + \begin{bmatrix} \cos \psi_s & \sin \psi_s & 0 \\ -\sin \psi_s & \cos \psi_s & 0 \\ 0 & 0 & 1 \end{bmatrix} \begin{bmatrix} 1 & 0 & 0 \\ 0 & \cos \phi_s & \sin \phi_s \\ 0 & -\sin \phi_s & \cos \phi_s \end{bmatrix} \begin{bmatrix} p \\ q \\ r \end{bmatrix} \quad (12)$$

$$\rightarrow \begin{cases} p_Y = (q \cos \phi_s + r \sin \phi_s) \sin \psi_s + (p + \dot{\phi}_s) \cos \psi_s \\ q_Y = (q \cos \phi_s + r \sin \phi_s) \cos \psi_s - (p + \dot{\phi}_s) \sin \psi_s \\ r_Y = (-q \sin \phi_s + r \cos \phi_s) + \dot{\psi}_s \end{cases}$$

Utilizing $[\omega^{BI}]^R$ and $[\omega^{RB}]^R$, the angular velocity vector of the outer frame relative to the inertial frame, and expressed in the outer frame, is calculated as follows:

$$\begin{bmatrix} \omega^{RI} \end{bmatrix}^R = \begin{bmatrix} \omega^{RB} \end{bmatrix}^R + [T]^{RB} \begin{bmatrix} \omega^{BI} \end{bmatrix}^B \quad (13)$$

$$\begin{bmatrix} p_R \\ q_R \\ r_R \end{bmatrix} = \begin{bmatrix} \dot{\phi}_s \\ 0 \\ 0 \end{bmatrix} + \begin{bmatrix} 1 & 0 & 0 \\ 0 & \cos \phi_s & \sin \phi_s \\ 0 & -\sin \phi_s & \cos \phi_s \end{bmatrix} \begin{bmatrix} p \\ q \\ r \end{bmatrix} \quad (14)$$

$$\rightarrow \begin{cases} p_R = p + \dot{\phi}_s \\ q_R = q \cos \phi_s + r \sin \phi_s \\ r_R = -q \sin \phi_s + r \cos \phi_s \end{cases}$$

Using Eq.(14), Eq. (12) can be simplified as(15):

$$\begin{cases} p_Y = q_R \sin \psi_s + p_R \cos \psi_s \\ q_Y = q_R \cos \psi_s - p_R \sin \psi_s \\ r_Y = r_R + \dot{\psi}_s \end{cases} \quad (15)$$

To obtain the equations of motion of the gimbals, Euler's laws have been used. I_I^{BI} is the angular momentum of the rigid body **B** WRT frame I and refers to its center of mass. Point I. it is calculated from the relation $I_B^{BI} = I_B^B \omega^{BI}$ where I_B^B is the moment of inertia tensor and ω^{BI} the angular velocity vector. In this case, it can be written [23]:

$$\mathbf{m}_B = D^I J_B^{BI} \quad (16)$$

In the above equation, \mathbf{m}_B is the external torque vector applied to the center of mass B. In an ideal condition, the seeker's moment of inertia matrix is diagonal and there is no mass imbalance. The torque components, required to rotate the gimbals are also expressed by and \mathbf{m}_R represent the torques required for the rotation of the inner gimbal and the outer gimbal, respectively. $[I_Y^Y]^Y$ is the moment of inertia matrix of the inner gimbal and $[I_R^R]^R$ is the moment of inertia matrix of the outer gimbal. These matrices are considered to be diagonal in ideal conditions:

$$\begin{bmatrix} I_R^R \end{bmatrix}^R = \begin{bmatrix} I_{Rx} & 0 & 0 \\ 0 & I_{Ry} & 0 \\ 0 & 0 & I_{Rz} \end{bmatrix}, \quad (17)$$

$$\begin{bmatrix} I_Y^Y \end{bmatrix}^Y = \begin{bmatrix} I_{Yx} & 0 & 0 \\ 0 & I_{Yy} & 0 \\ 0 & 0 & I_{Yz} \end{bmatrix}$$

In the following, the dynamic equations of the inner and outer gimbal are obtained by assuming the center of P and R frames to be the same. For the rotational dynamics governing the inner gimbal, the Euler's law is written as [23]:

$$\begin{aligned} \left[\sum \mathbf{m}_Y \right]^Y &= \begin{bmatrix} m_{Yx} & m_{Yy} & m_{Yz} \end{bmatrix}^T = \\ \left[\mathbf{I}_Y^Y \right]^Y \left[\frac{d\boldsymbol{\omega}^{YI}}{dt} \right]^Y &+ \left[\boldsymbol{\Omega}^{YI} \right]^Y \left[\mathbf{I}_Y^Y \right]^Y \left[\boldsymbol{\omega}^{YI} \right]^Y \end{aligned} \quad (18)$$

In above equation, $\boldsymbol{\Omega}^{YI}$ is the angular velocity tensor of frame Y relative to frame I. The expansion of this relationship is as follows:

$$\begin{aligned} \left[\sum \mathbf{m}_Y \right]^Y &= \begin{bmatrix} I_{Yx} & 0 & 0 \\ 0 & I_{Yy} & 0 \\ 0 & 0 & I_{Yz} \end{bmatrix} \begin{bmatrix} \dot{p}_Y \\ \dot{q}_Y \\ \dot{r}_Y \end{bmatrix} + \\ \begin{bmatrix} 0 & -r_Y & q_Y \\ r_Y & 0 & -p_Y \\ -q_Y & p_Y & 0 \end{bmatrix} \begin{bmatrix} I_{Yx} p_Y \\ I_{Yy} q_Y \\ I_{Yz} r_Y \end{bmatrix} &= \quad (19) \\ \begin{bmatrix} I_{Yx} \dot{p}_Y - I_{Yy} q_Y r_Y + I_{Yz} r_Y q_Y \\ I_{Yy} \dot{q}_Y + I_{Yx} p_Y r_Y - I_{Yz} r_Y p_Y \\ I_{Yz} \dot{r}_Y - I_{Yx} p_Y q_Y + I_{Yy} q_Y p_Y \end{bmatrix} \end{aligned}$$

Since the inner gimbal only rotates around the z-axis, the third component of Eq. (19) is used as the equation governing the rotation of the inner gimbal.

$$m_{Yz} = I_{Yz} \dot{r}_Y + p_Y q_Y (I_{Yy} - I_{Yx}) \quad (20)$$

As a result:

$$\dot{r}_Y = \frac{m_{Yz} + p_Y q_Y (I_{Yx} - I_{Yy})}{I_{Yz}} \quad (21)$$

By defining $T_{d_{yaw}} = p_Y q_Y (I_{Yx} - I_{Yy})$, Eq. (21) is rewritten in the following form:

$$\dot{r}_Y = \frac{m_{Yz} + T_{d_{yaw}}}{I_{Yz}} \quad (22)$$

For the rotational dynamics governing the outer gimbal, it

can be written according to Euler's law:

$$\mathbf{m}_R = D^I \mathbf{I}_R^{RI} = D^I (\mathbf{I}_R^R \boldsymbol{\omega}^{RI}) \quad (23)$$

$$\begin{aligned} \left[\sum \mathbf{m}_R \right]^R &= \begin{bmatrix} m_{Rx} & m_{Ry} & m_{Rz} \end{bmatrix}^T = \\ \left[\mathbf{I}_R^R \right]^R \left[\frac{d\boldsymbol{\omega}^{RI}}{dt} \right]^R &+ \left[\boldsymbol{\Omega}^{RI} \right]^R \left[\mathbf{I}_R^R \right]^R \left[\boldsymbol{\omega}^{RI} \right]^R \end{aligned} \quad (24)$$

The angular momentum of the outer gimbal consists of two parts. One part is related to the angular momentum of the outer gimbal, and the other is due to the angular momentum of the inner gimbal. The angular momentum of the outer gimbal is expressed using the transformation matrix $[T]^{RP}$ in the inner frame.

$$\begin{aligned} \left[\mathbf{I}_R^{RI} \right]^R &= \begin{bmatrix} I_{Rx} \\ I_{Ry} \\ I_{Rz} \end{bmatrix} = \left[\mathbf{I}_R^{RI} \right]^R + [T]^{RY} \left[\mathbf{I}_Y^{YI} \right]^Y = \\ \left[\mathbf{I}_R^R \right]^R \left[\boldsymbol{\omega}^{RI} \right]^R &+ [T]^{RY} \left[\mathbf{I}_Y^Y \right]^Y \left[\boldsymbol{\omega}^{YI} \right]^Y \end{aligned} \quad (25)$$

By inserting Eq. (25) into Eq. (24), external torques applied on the center of mass R are obtained. Since the outer gimbal only rotates around the X-axis, the first component of Eq. (23) is used as the outer gimbal equation of motion.

$$\begin{aligned} m_{Rx} &= (\dot{p}_Y I_{Yx} \cos \psi_s - \dot{q}_Y I_{Yy} \sin \psi_s \\ &+ I_{Rx} \dot{p}_R - p_Y I_{Yx} \sin \psi_s \dot{\psi}_s - q_Y I_{Yy} \cos \psi_s \dot{\psi}_s) \\ &- r_R (p_Y I_{Yx} \sin \psi_s + q_Y I_{Yy} \cos \psi_s + I_{Ry} q_R) \\ &+ q_R (r_Y I_{Yz} + I_{Rz} r_R) \end{aligned} \quad (26)$$

Both \dot{p}_Y and \dot{q}_Y are obtained from the derivative of the first and second components of Eq. (15):

$$\begin{cases} \dot{p}_Y = \dot{q}_R \sin \psi_s + \dot{p}_R \cos \psi_s \\ \quad + q_R \cos \psi_s \dot{\psi}_s - p_R \sin \psi_s \dot{\psi}_s \\ \dot{q}_Y = \dot{q}_R \cos \psi_s - \dot{p}_R \sin \psi_s \\ \quad - q_R \sin \psi_s \dot{\psi}_s - p_R \cos \psi_s \dot{\psi}_s \end{cases} \quad (27)$$

The component \dot{q}_R is calculated by the derivative of the second component of Eq. (14):

$$\begin{aligned} \dot{q}_R &= \dot{q} \cos \varphi_s + \dot{r} \sin \varphi_s \\ &\quad - q \sin \varphi_s \dot{\varphi}_s + r \cos \varphi_s \dot{\varphi}_s \end{aligned} \quad (28)$$

By substituting Eqs. (27) and (28) into Eq.(26) we have:

$$\begin{aligned} m_{R_x} &= I_{Y_x} \cos \psi_s [\sin \psi_s (\dot{q} \cos \varphi_s + \dot{r} \sin \varphi_s \\ &\quad - q \sin \varphi_s \dot{\varphi}_s + r \cos \varphi_s \dot{\varphi}_s) + \\ &\quad \dot{p}_R \cos \psi_s + q_R \cos \psi_s \dot{\psi}_s - p_R \sin \psi_s \dot{\psi}_s] \\ &\quad - I_{Y_y} \sin \psi_s [\cos \psi_s (\dot{q} \cos \varphi_s + \dot{r} \sin \varphi_s \\ &\quad - q \sin \varphi_s \dot{\varphi}_s + r \cos \varphi_s \dot{\varphi}_s) \\ &\quad - \dot{p}_R \sin \psi_s - q_R \sin \psi_s \dot{\psi}_s - p_R \cos \psi_s \dot{\psi}_s] \\ &\quad + I_{R_x} \dot{p}_R - p_Y I_{Y_x} \sin \psi_s \dot{\psi}_s - q_Y I_{Y_y} \cos \psi_s \dot{\psi}_s \\ &\quad - r_R (p_Y I_{Y_x} \sin \psi_s + q_Y I_{Y_y} \cos \psi_s + I_{R_y} q_R) \\ &\quad + q_R (r_Y I_{Y_z} + I_{R_z} r_R) \end{aligned} \quad (29)$$

Considering the \dot{p}_R coefficients as the equivalent moment of inertia, we would have:

$$I_{eq} = I_{R_x} + I_{Y_x} \cos^2 \psi_s + I_{Y_y} \sin^2 \psi_s \quad (30)$$

Now define T_{d1} and T_{d2} as follows:

$$\begin{aligned} T_{d1} &= -I_{Y_x} \cos \psi_s (q_R \cos \psi_s - p_R \sin \psi_s) \\ &\quad + I_{Y_y} \sin \psi_s (-q_R \sin \psi_s - p_R \cos \psi_s) \\ &\quad + p_Y I_{Y_x} \sin \psi_s + q_Y I_{Y_y} \cos \psi_s \end{aligned} \quad (31)$$

$$\begin{aligned} T_{d2} &= -I_{Y_x} \cos \psi_s [\sin \psi_s (\dot{q} \cos \varphi_s + \dot{r} \sin \varphi_s \\ &\quad - q \sin \varphi_s \dot{\varphi}_s + r \cos \varphi_s \dot{\varphi}_s) \\ &\quad + I_{Y_y} \sin \psi_s [\cos \psi_s (\dot{q} \cos \varphi_s + \dot{r} \sin \varphi_s \\ &\quad - q \sin \varphi_s \dot{\varphi}_s + r \cos \varphi_s \dot{\varphi}_s) \\ &\quad + r_R (p_Y I_{Y_x} \sin \psi_s + q_Y I_{Y_y} \cos \psi_s + I_{R_y} q_R) \\ &\quad - q_R (r_Y I_{Y_z} + I_{R_z} r_R) \end{aligned} \quad (32)$$

Substituting Eq. (30-32) into Eq. (31), we would have:

$$I_{eq} \dot{p}_R = m_{R_x} + T_{d1} \dot{\psi}_s + T_{d2} \quad (33)$$

$$\dot{p}_R = \frac{T_{d1}}{I_{eq}} (r_p - r_R) + \frac{1}{I_{eq}} (m_{R_x} + T_{d2}) \quad (34)$$

If a rate gyro is mounted along the x_Y axis of the inner gimbal, it measures the \dot{p}_Y . According to the first component of Eq. (27), Eq. (28) is rewritten as follows:

$$\dot{p}_Y = \dot{p}_R \cos \psi_s - (-\dot{q}_R \sin \psi_s - q_Y \dot{\psi}_s) \quad (35)$$

Now define T_{dRoll} as:

$$\begin{aligned} T_{dRoll} &= \cos \psi_s (T_{d1} \dot{\psi}_s + T_{d2}) \\ &\quad - I_{eq} (-\dot{q}_R \sin \psi_s - q_Y (r_Y - r_R)) \end{aligned} \quad (36)$$

According to Eq. (35) is rewritten as follows:

$$\dot{p}_Y = \frac{\cos \psi_s m_{R_x} + T_{dRoll}}{I_{eq}} \quad (37)$$

The block diagram of Figure 4 shows the seeker's roll and yaw channels, in which Eq. (22) is used in the yaw channel and Eq. (37) in the roll channel. It should be noted that the roll channel, after calculating p_Y , p_R is calculated according to the first component of relation (15).

4- Sliding Mode Control of Roll-yaw Seeker

The Roll-yaw seeker dynamic derived in Section 2 is a nonlinear dynamic with strong coupling. Also, mass unbalances and disturbances lead to uncertainty in the model. Uncertainty can cause undesirable system performance. In this part, the sliding mode controller controls this nonlinear uncertain system. In the following, the control structure of the roll-yaw seeker, which includes the stabilization loop and the tracking loop, is introduced and analyzed by separating the roll and yaw channels. A method is presented to solve the singularity problem in the tracking loop by analyzing it. Then, the sliding mode controller is introduced and used to control the roll-yaw seeker nonlinear system. In a roll-yaw seeker, model uncertainties (e.g., gimbal inertia mismatches, cross-axis coupling, unmodeled actuator dynamics) and frictional moments (e.g., static, Coulomb, and viscous friction) significantly impact performance by causing tracking errors, instability, and mechanical wear. Integral Sliding Mode Control (ISMC) effectively addresses these challenges by combining robust disturbance rejection with integral action to eliminate steady-state errors caused by uncertainties or friction. The control law incorporates switching terms to

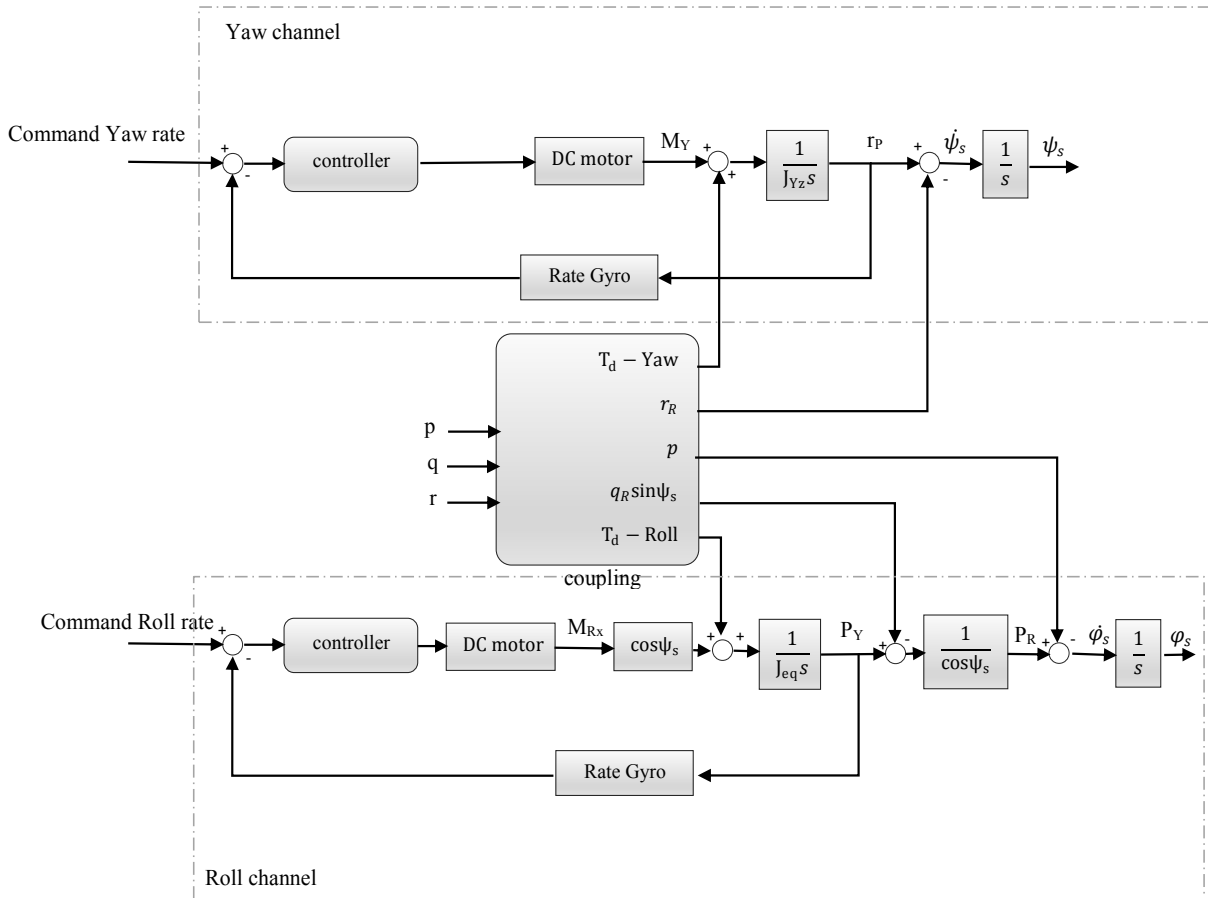


Fig. 4. Block diagram of roll and yaw channels

handle bounded disturbances and a boundary layer (e.g., saturation function) to reduce chattering and mitigate stick-slip effects. Independent sliding surfaces for roll and pitch axes ensure robustness against cross-coupling, while adaptive compensation and simulation-based tuning improve reliability under varying conditions. ISMC's robustness and smooth control make it ideal for precise and reliable target tracking in roll-yaw seekers.

4- 1- Stabilization loop

In the stabilization loop, there are two main control objectives. The first goal is to stabilize the inner frame in the inertial space. Sensors are also installed on the inner frame of the seeker. The sensors being fixed in the inertial space calculate the error angles independently of the disturbance moments. The second purpose is to track the desired roll and yaw angular velocities produced in the tracking loop by the inner frame. The controller designed for the stabilization loop is the integral sliding mode control, which is also designed in this section.

4- 2- Tracking loop

In the tracking loop, the tracking error should reach zero. In other words, in this loop, the seeker's head is placed along the LOS vector expressed in the inner frame. For this purpose, first, the roll error and yaw error required by the axes of the seeker must be positioned toward the target. These errors are calculated from Eqs. (4) and (5). Then, the rotation rate command is required to regulate the angular error in the roll and yaw channels, which are sent to the stabilization loop. In the stabilization loop, for the X_p axis of the seeker to face the target, the desired torque is generated and applied to the frames to rotate the roll and yaw frames, and then the target is tracked. It should be considered that the tracking error is proportional to the detector output. The detector's task is to identify and express the target's position. The detector output is the elevation and azimuth angles of the target relative to the seeker and is expressed in its inner frame. The roll and yaw errors are calculated according to the elevation and azimuth angles by converting from the Cartesian coordinate system to the polar one. The roll and yaw errors are the control inputs of the roll and yaw channels of the tracking loop, respectively.

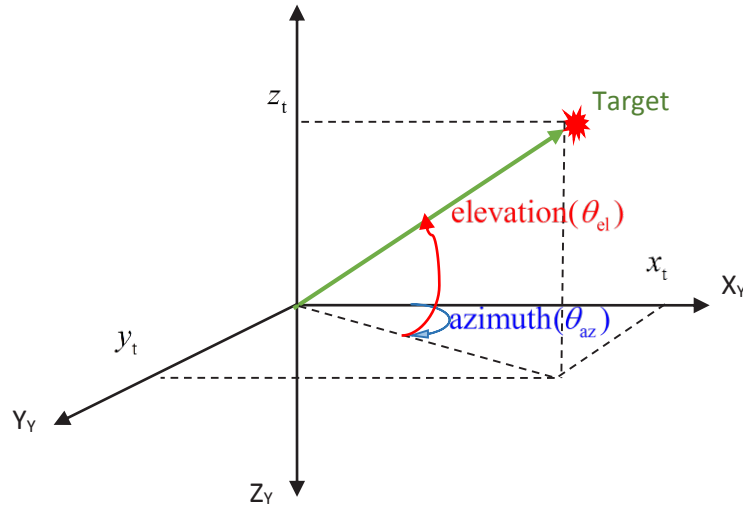


Fig. 5. The position of the target relative to the inner frame expressed by elevation and azimuth angles

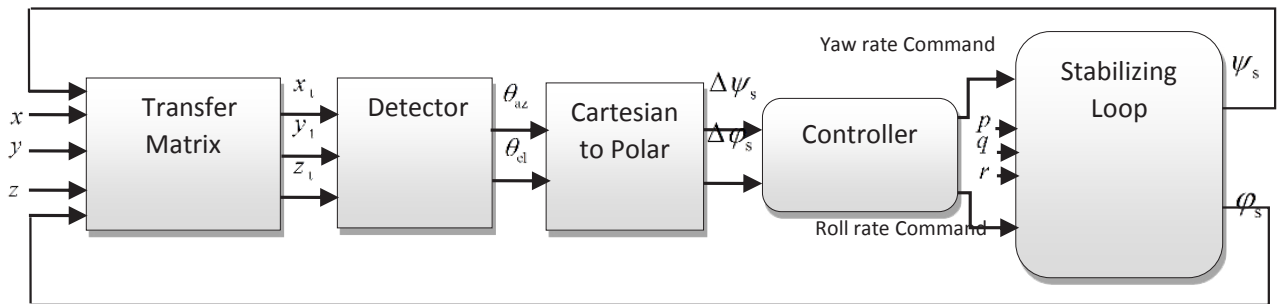


Fig. 6. The block diagram of the tracking loop

According to Figure 5, the elevation and azimuth angles are indicated by θ_{el} and θ_{az} respectively.

Consider that always $x_t \geq 0$, the variables x_t , y_t and z_t , are rewritten as follows:

$$\begin{cases} x_t = x_t \\ y_t = x_t \tan \theta_{az} \\ z_t = -x_t \sqrt{1 + \tan^2 \theta_{az}} \tan \theta_{el} \end{cases} \quad (38)$$

According to Eq. (38), the roll and yaw error values are obtained according to the elevation and azimuth errors. The block diagram of the tracking loop considering the roll and yaw channels is shown in Figure 6:

Yaw channel

Using Eq. (5) and (38) and noting that x_t is positive, the seeker yaw error is proportional to the information received from the detector as follows:

$$\Delta\psi_s = \tan^{-1}(\text{sgn}(\tan \theta_{az}) \times \sqrt{(-\sqrt{1 + \tan^2 \theta_{az}} \tan \theta_{el})^2 + (\tan \theta_{az})^2}) \quad (39)$$

Using a proportional controller by gain k_p , the desired yaw rate command is generated and input to the yaw channel stabilization loop.

Roll channel

using relations (4) and (38), the seeker roll error is proportional to the elevation and azimuth angles as follows:

$$\Delta\varphi_s = \tan^{-1}\left(\frac{-\sqrt{1 + \tan^2 \theta_{az}} \tan \theta_{el}}{\tan \theta_{az}}\right) \quad (40)$$

Designing a proportional controller by gain k_{p_s} , the roll rate command is generated and fed into the roll channel stabilization loop. In the roll channel, when the X axis of the inner frame (X_Y) faces the target, the roll rate becomes infinite and a singularity occurs. The following will discuss the investigation and solution to remove this singularity.

Roll channel singularity

To obtain the roll and pitch rate according to Eqs. (4) and (5), we can write:

$$\begin{cases} \tan \Delta\varphi_s = \frac{z_t}{y_t} \\ \tan \Delta\psi_s = \text{sgn}(y_t) \frac{\sqrt{z_t^2 + y_t^2}}{x_t} \end{cases} \quad (41)$$

By differentiation from the Eq. (41), the following equation will be obtained:

$$\begin{cases} \frac{1}{\cos^2 \Delta\varphi_s} \Delta\dot{\varphi}_s = \frac{\dot{z}_t y_t - \dot{y}_t z_t}{y_t^2} \\ \frac{1}{\cos^2 \Delta\psi_s} \Delta\dot{\psi}_s = \frac{(z_t^2 + y_t^2)^{-0.5} (z_t \dot{z}_t + y_t \dot{y}_t) x_t - (z_t^2 + y_t^2)^{0.5} \dot{x}_t}{x_t^2} \text{sgn}(y_t) \end{cases} \quad (42)$$

In Eq. (42) the $\text{sgn}(y_t)$ derivative at the point $y_t = 0$ is undefined. According to Eq. (42), the relations of roll rate and pitch rate is as follows:

$$\begin{cases} \Delta\dot{\varphi}_s = \frac{\dot{z}_t y_t - \dot{y}_t z_t}{y_t^2} \cos^2 \Delta\varphi_s \\ \Delta\dot{\psi}_s = \frac{(z_t^2 + y_t^2)^{-0.5} (z_t \dot{z}_t + y_t \dot{y}_t) x_t - (z_t^2 + y_t^2)^{0.5} \dot{x}_t}{x_t^2} \times \text{sgn}(y_t) \cos^2 \Delta\psi_s \end{cases} \quad (43)$$

According to Figure 3, the trigonometric functions are obtained in the following equations:

$$\begin{cases} \cos \Delta\varphi_s = \frac{y_t}{\sqrt{y_t^2 + z_t^2}} \\ \cos \Delta\psi_s = \frac{x_t}{\sqrt{z_t^2 + y_t^2 + x_t^2}} \end{cases} \Rightarrow \quad (44)$$

$$\begin{cases} \cos^2 \Delta\varphi_s = \frac{y_t^2}{y_t^2 + z_t^2} \\ \cos^2 \Delta\psi_s = \frac{x_t^2}{z_t^2 + y_t^2 + x_t^2} \end{cases}$$

$$\begin{cases} \sin \Delta\varphi_s = \frac{z_t}{\sqrt{y_t^2 + z_t^2}} \\ \sin \Delta\psi_s = \frac{\sqrt{y_t^2 + z_t^2}}{\sqrt{z_t^2 + y_t^2 + x_t^2}} \text{sgn}(y_t) \end{cases} \Rightarrow \quad (45)$$

$$\begin{cases} \sqrt{y_t^2 + z_t^2} \sin \Delta\varphi_s = z_t \\ \sqrt{z_t^2 + y_t^2 + x_t^2} \sin \Delta\psi_s = \sqrt{y_t^2 + z_t^2} \text{sgn}(y_t) \end{cases}$$

Replacing Eq. (44) in Eq. (43) we would have:

$$\left\{ \begin{aligned} \begin{bmatrix} \Delta\dot{\phi}_s \\ \Delta\dot{\psi}_s \end{bmatrix} &= \begin{bmatrix} 0 & \frac{-z_t}{y_t^2+z_t^2} & \frac{y_t}{y_t^2+z_t^2} \\ \frac{-(z_t^2+y_t^2)^{0.5}}{z_t^2+y_t^2+x_t^2} \text{sgn}(y_t) & \frac{(z_t^2+y_t^2)^{-0.5} y_t x_t}{z_t^2+y_t^2+x_t^2} \text{sgn}(y_t) & \frac{(z_t^2+y_t^2)^{-0.5} z_t x_t}{z_t^2+y_t^2+x_t^2} \text{sgn}(y_t) \end{bmatrix} \begin{bmatrix} \dot{x}_t \\ \dot{y}_t \\ \dot{z}_t \end{bmatrix} \\ \mathbf{k} &= \begin{bmatrix} 0 & \frac{-\sin \Delta\phi_s}{\sqrt{y_t^2+z_t^2}} & \frac{\cos \Delta\phi_s}{\sqrt{y_t^2+z_t^2}} \\ \frac{\sin \Delta\psi_s}{\sqrt{z_t^2+y_t^2+x_t^2}} & \frac{\cos \Delta\phi_s \cos \Delta\psi_s}{\sqrt{z_t^2+y_t^2+x_t^2}} \text{sgn}(y_t) & \frac{\sin \Delta\phi_s \cos \Delta\psi_s}{\sqrt{z_t^2+y_t^2+x_t^2}} \text{sgn}(y_t) \end{bmatrix} \end{aligned} \right. \quad (46)$$

Considering $y_t \rightarrow 0$, $z_t \rightarrow 0$ and $x_t \neq 0$; It is clear that the $\Delta\dot{\phi}_s$ coefficients (the first row of the matrix \mathbf{k} in Eq. (46)) become infinite. Also, with the assumption that the distance between the target and the seeker is large, the limit of the matrix \mathbf{k} as $y_t \rightarrow 0$, $x_t \rightarrow \infty$ and $z_t \rightarrow 0$ is obtained as follows:

$$\lim_{\substack{x_t \rightarrow \infty \\ y_t \rightarrow 0 \\ z_t \rightarrow 0}} \mathbf{k} = \begin{bmatrix} 0 & \infty & \infty \\ 0 & 0 & 0 \end{bmatrix} \quad (47)$$

Due to Eq. (47), when the seeker's head is facing the target, the rotation roll rate becomes infinite and causes a singularity.

4- 3- Roll channel singularity avoidance

As stated in the previous section, singularity occurs when the x-axis of the seeker's inner frame is facing the target. This means the target position with the values $y_t \rightarrow 0$, $z_t \rightarrow 0$

and $x_t \neq 0$ in the inner frame. The origin of the singularity is Eq. (40), which expresses the roll kinematics in terms of the detector output. According to Figure 6 and Eq. (40), it is clear that the singularity problem occurs in the cartesian to polar transfer function block. Eqs. (39) and (40), which are embedded in this block are roll and yaw errors proportional to elevation and azimuth errors, respectively.

Since the error values in both roll and yaw channels in the tracking loop are small (because the seeker starts working in the final phase of the flight and after locking on the target), the detector outputs can be considered directly as the input of the tracking loop controller. For this purpose, the azimuth error is considered the input command of the yaw control loop, and the elevation error is considered the input command of the roll control loop. This idea is inspired by the bank-to-turn model of an aircraft, where a roll command is issued if there is an azimuth error. In this way, there is no singularity in the proposed method due to not using Eq. (40).

In Figure 7, (a) shows the tracking error in the presence of elevation and azimuth error, and (b) shows the tracking error after regulating the elevation error by rotating around

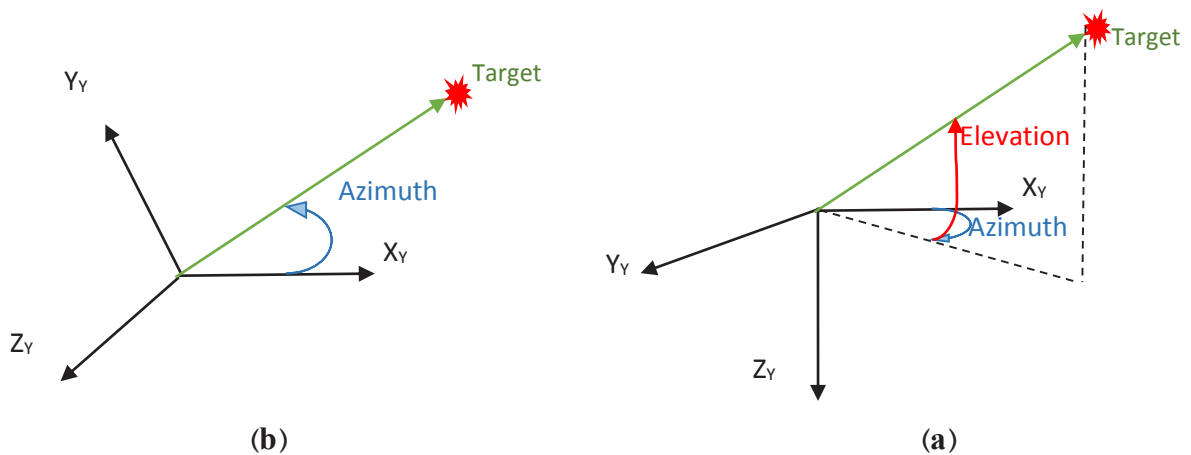


Fig. 7. The position of the target relative to the inner frame expressed by elevation and azimuth angles

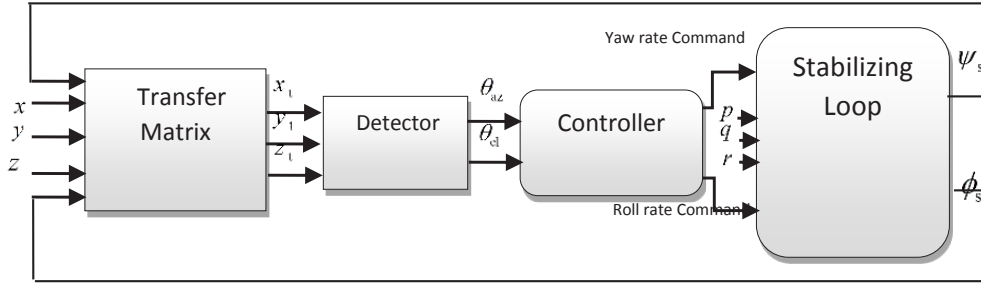


Fig. 8. Block diagram of the tracking loop with singularity avoidance

the Xp axis.

In the roll-yaw seeker, to reduce the pitch error to zero, the seeker rolls proportional to the elevation error. As a result, the LOS vector is placed in the X-Y plane (Figure 7). If the elevation error is small enough, the azimuth error will equal the seeker's yaw error. In this way, the tracking error becomes zero. The block diagram of the tracking loop with singularity correction is shown in Figure 8.

4- 4- Integrated sliding mode

The sliding mode controller design is done in two steps. The first step is to define the stable sliding surface. So, if the system's state is placed on the sliding surface, it remains on it and tends to the equilibrium state by moving on the sliding surface. There are sliding surfaces as many as control inputs. The second step is to design the control law that directs the system's state toward the sliding surface $s(\mathbf{x}, t) = 0$ at any moment.

The roll-yaw seeker has two control inputs. Therefore, the sliding mode controller design is done for a multi-input-multi-output system. On the other hand, the chattering in this control method is undesirable for a seeker and should be removed. To remove the chattering, an optional error must be considered for the system. This error is eliminated by using the integral sliding mode controller. In the following, the integral sliding mode controller, a two-input-two-output system, is designed for roll-yaw seeker stabilization loops.

The coupling between the roll and yaw channels is described in the second section under the names $T_{d_{Roll}}$ and $T_{d_{Yaw}}$. This coupling is described in the controller design as $d_{Roll}(x)$ and $d_{Yaw}(x)$ which is entered into the controller equation as a disturbance. In this way, the coupling between the two roll and yaw channels is already provided in the controller design and this robust controller greatly reduces the effect of the coupling. According to Eqs. (22) and (37), $T_{d_{Yaw}}$ and $T_{d_{Roll}}$ are considered as disturbance inputs. The dynamic equations are rewritten as follows:

$$\begin{cases} \dot{x}_1 = b_{Yaw}(x)u + d_{Yaw}(x) \Rightarrow \\ \left\{ \begin{aligned} d_{Yaw}(x) &= \frac{T_{d_{Yaw}}}{I_{YZ}}, b_{Yaw}(x) = \frac{1}{I_{YZ}} \end{aligned} \right. \\ \\ \dot{x}_2 = b_{Roll}(x)u + d_{Roll}(x) \Rightarrow \\ \left\{ \begin{aligned} d_{Roll}(x) &= \frac{T_{d_{Roll}}}{I_{eq}}, b_{Roll}(x) = \frac{\cos \psi_s}{I_{eq}} \end{aligned} \right. \end{cases} \quad (48)$$

To design the control signal, the uncertainty limit is assumed as follows:

$$\begin{cases} \dot{x} = b(x)u + d(x) \Rightarrow \begin{cases} 0 \leq b^- \leq b \leq b^+ \\ \hat{b} = \sqrt{b^+ b^-} \end{cases}, \\ y = x \\ \beta = \sqrt{\frac{b^+}{b^-}}, |d| \leq \delta(x, t) \end{cases} \quad (49)$$

in which β is the gain margin and $\delta(x, t)$ is the disturbances limit. Since the control variable is the integral error, the equation increases by one order.

$$\int \ddot{x} = \dot{x} = b(x)u + d(x) \rightarrow n = 2 \quad (50)$$

The order for the system is 2. The sliding surface is defined as follows:

$$\begin{cases} s(\mathbf{x}, t) = \left(\frac{d}{dt} + \lambda\right) \int_0^t e = e + \lambda \int e \Rightarrow \\ \dot{s}(\mathbf{x}, t) = \dot{e} + \lambda e = 0 \end{cases} \quad (51)$$

By solving the \dot{s} in terms of control input, the equivalent control is obtained which is shown by u_{eq} . It is a continuous control law that maintains $\dot{s}(\mathbf{x}, t) = 0$ when the exact dynamics are known. The sliding mode control signal is as the following [25]:

$$u = u_{eq} - k\hat{b}^{-1} \text{sgn}(s) = \hat{b}^{-1}(\hat{u} - k \text{sgn}(s)) \quad (52)$$

where k is the coefficient of the sign function obtained from the sliding condition. The sliding condition is as follows [25]:

$$s\dot{s} \leq -\eta |s| \quad (53)$$

Putting \dot{s} in the sliding condition, the allowable interval for k is obtained:

$$\begin{aligned} s\dot{s} &= s(bu + d - \dot{x}_d + \lambda e) = \\ &= s(b(\hat{b}^{-1}(\dot{x}_d - \lambda e - k \text{sgn}(s))) + d - \dot{x}_d + \lambda e) = \\ &= s(b\hat{b}^{-1}\dot{x}_d - b\hat{b}^{-1}\lambda e - b\hat{b}^{-1}k \text{sgn}(s) + d - \dot{x}_d + \lambda e) = \\ &= s((b\hat{b}^{-1} - 1)\dot{x}_d + (1 - b\hat{b}^{-1})\lambda e - b\hat{b}^{-1}k \text{sgn}(s) + d) \end{aligned} \quad (54)$$

Factoring from $-(1 - b\hat{b}^{-1})$ and considering $\text{sgn}(s) = \frac{|s|}{s}$, we would have:

$$\begin{aligned} &s(1 - b\hat{b}^{-1})(\dot{x}_d - \lambda e) - b\hat{b}^{-1}k |s| + sd = \\ &s(1 - b\hat{b}^{-1})\hat{u} - b\hat{b}^{-1}k |s| + sd \end{aligned} \quad (55)$$

Using the triangle inequality leads to:

$$s\dot{s} \leq |s| |1 - b\hat{b}^{-1}| |\hat{u}| - b\hat{b}^{-1}k |s| + |s| d \quad (56)$$

Considering $d \leq \delta$ and also Eq. (49), the second expression on the right side of Eq. (56) can be written as:

$$\beta^{-1} \leq b\hat{b}^{-1} \leq \beta \Rightarrow -b\hat{b}^{-1} \leq -\beta^{-1} \quad (57)$$

Also, for the first term on the right-hand side of the inequality of Eq. (56), it can be said that:

$$\begin{cases} |1 - b\hat{b}^{-1}| \leq |1 - \beta^{-1}| \\ \beta = \sqrt{\frac{b^+}{b^-}} \geq 1 \Rightarrow 0 \leq \beta^{-1} \leq 1 \\ \rightarrow |1 - \beta^{-1}| = 1 - \beta^{-1} \end{cases} \Rightarrow \quad (58)$$

$$|1 - b\hat{b}^{-1}| \leq 1 - \beta^{-1}$$

Inequality (56) is rewritten as follows:

$$s\dot{s} \leq |s| (|1 - \beta^{-1}| |\hat{u}| - \beta^{-1}k + \delta) \quad (59)$$

Using the sliding condition, the proper interval for K is obtained:

$$\begin{aligned} &|s| (|1 - \beta^{-1}| |\hat{u}| - \beta^{-1}k + \delta) \leq -\eta |s| \\ &\rightarrow k \geq (\beta - 1) |\hat{u}| + \beta(\delta + \eta) \end{aligned} \quad (60)$$

The parameter K has a direct effect on the chattering. To remove chattering, $\tanh(\frac{s}{\phi})$ is used instead of $\text{sgn}(s)$ where ϕ is the boundary layer thickness. The control signal of two roll and yaw channels is rewritten as follows:

$$\begin{cases} u_{Yaw} = u_{eq_{Yaw}} - k_{Yaw} \hat{b}_{Yaw}^{-1} \tanh\left(\frac{S_{Yaw}}{\phi}\right) = \\ \hat{b}_{Yaw}^{-1} (\hat{u}_{Yaw} - k_{Yaw} \tanh\left(\frac{S_{Yaw}}{\phi}\right)) \\ u_{Roll} = u_{eq_{Roll}} - k_{Roll} \hat{b}_{Roll}^{-1} \tanh\left(\frac{S_{Roll}}{\phi}\right) = \\ \hat{b}_{Roll}^{-1} (\hat{u}_{Roll} - k_{Roll} \tanh\left(\frac{S_{Roll}}{\phi}\right)) \end{cases} \quad (61)$$

5- Numerical Simulation

In this section, the tracking loop simulation results are presented. In the tracking loop, the seeker is controlled so that its X_y axis is directed towards the target. In this test, the target is assumed at $x = 10000$, $y = 500$, and $z = 500$, and the error of $\Delta\varphi_s$ and $\Delta\psi_s$ is expected to be zero. To determine the control gains, first, using equation (60), the gain selection

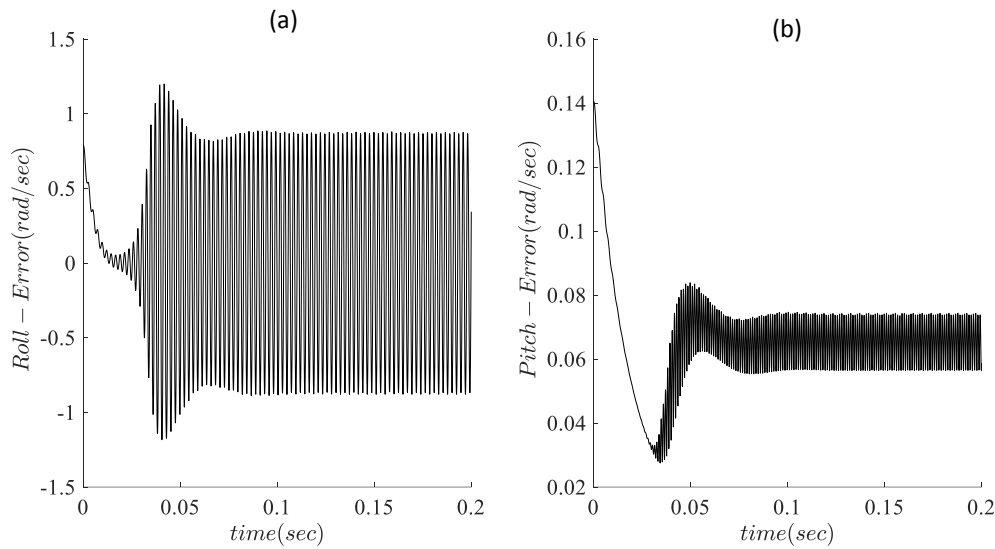


Fig. 9. The angular error of the target and the seeker XY axis despite the singularity

range for the system was calculated. Then, by considering the upper limit of the control gains and applying a trial and error approach, the lowest gain value that would ensure the desired performance of the system and prevent excessive control effort was selected. Since the presence of chattering in highly sensitive systems, such as seekers, is undesirable, its elimination is necessary. For this purpose, a boundary layer was defined in which the chattering is limited and will not be visible in the controller output. Since the application of this layer can lead to systematic error, its thickness was chosen in such a way that it eliminates chattering and creates the minimum possible error. All the simulation parameters are presented in the Appendix.

To clarify the singularity, the tracking loop simulation has been implemented despite the singularity and without considering the saturation limit of the input voltage and output current of the motor. Figure 9 shows the time response graphs of the angular error of the target and the seeker X_Y axis.

Figure 9 shows the angular error of the target and the seeker X_Y axis in the tracking loop, despite the singularity and without considering the saturations on the motor simulation. (a) is the roll error, and (b) is the yaw error.

To show the singularity in different scenarios, four different target positions were chosen and simulation has been implemented. Figure 10 shows the time response graphs of the angular error of the target and the seeker X_Y axis.

Figure 10 shows the angular error of the target and the seeker X_Y axis in the tracking loop, despite the singularity and without considering the saturations on the motor simulation. As is clear in these scenarios, wherever the target position is, the seeker axis rotates towards the target, and as soon as

the yaw error becomes zero and the seeker axis is positioned opposite the target, the roll angle becomes infinite and the singularity occurs. In this figure, in scenario (1) target is assumed at $x = 10000$, $y = 0$, and $z = -500$, in scenario (2) target is assumed at $x = 10000$, $y = 500$, and $z = -500$, in scenario (3) target is assumed at $x = 10000$, $y = -500$, and $z = -500$, in scenario (4) target is assumed at $x = 10000$, $y = -500$, and $z = 500$, and the error of $\Delta\varphi_s$ and $\Delta\psi_s$ are expected to be zero. And in all of the scenarios (a) is the roll error, and (b) is the yaw error.

In the following, the tracking loop simulation has been implemented after the singularity avoidance. Figure 11 shows the time response graphs of the angular error of the target and the seeker X_Y axis. According to the graphs, the singularity problem has been entirely resolved, and with zero error, the seeker's head has turned towards the assumed target.

Figure 11 shows the angular error of the target and the seeker X_Y axis in the tracking loop, by singularity avoidance. (a) is the elevation error, and (b) is the azimuth error.

The tracking loop simulation after the singularity avoidance in the presence of $[-50\% \ 100\%]$ uncertainty in the moment of inertia is shown in Figure 12. As can be seen, the designed sliding mode controller tracks the desired values very well in the presence of uncertainty. Also, according to the uncertainty interval, it is clear that the controller's sensitivity to this parameter is very low, and the controller is resistant to the uncertainty in the moment of inertia matrix.

Figure 12 shows the angular error of the target and the seeker X_Y axis in the tracking loop, by singularity avoidance in the presence of $[-50\% \ 100\%]$ uncertainty. (a) is the elevation error, and (b) is the azimuth error.

In order to further validate the controller, the seeker

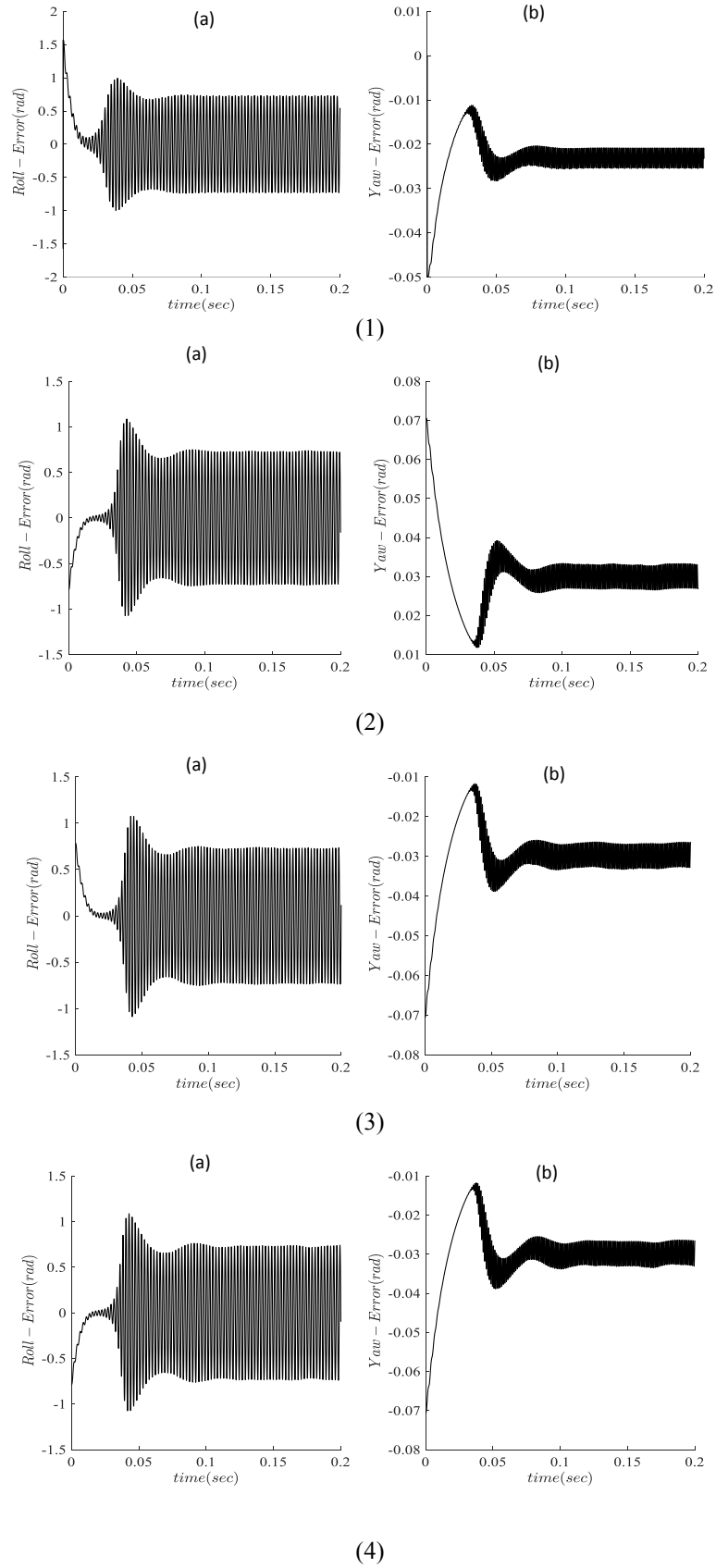


Fig. 10. The angular error of the target and the seeker XY axis despite the singularity in other scenarios

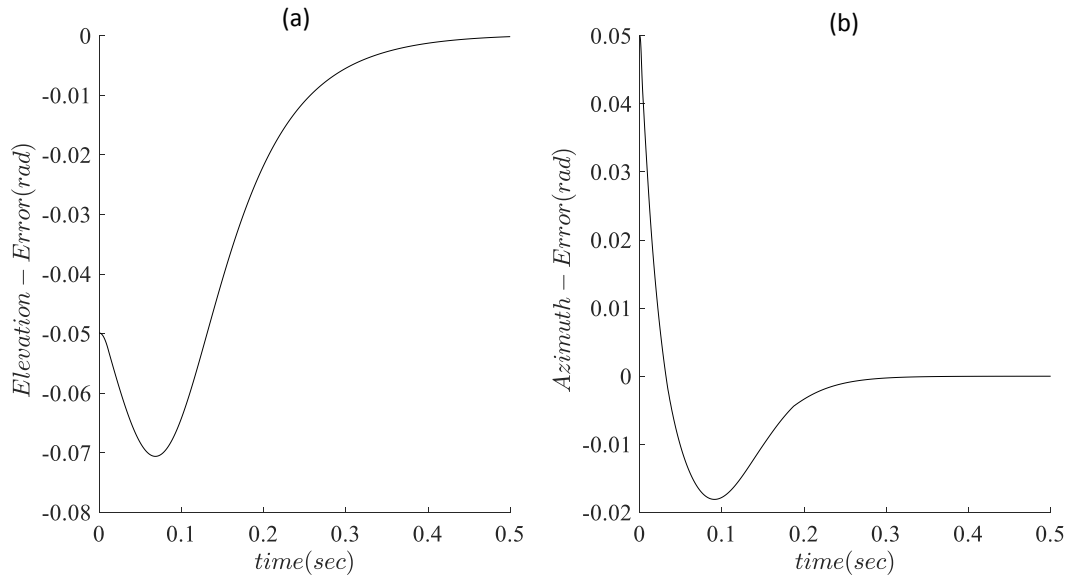


Fig. 11. The angular error of the target and the seeker by singularity avoidance

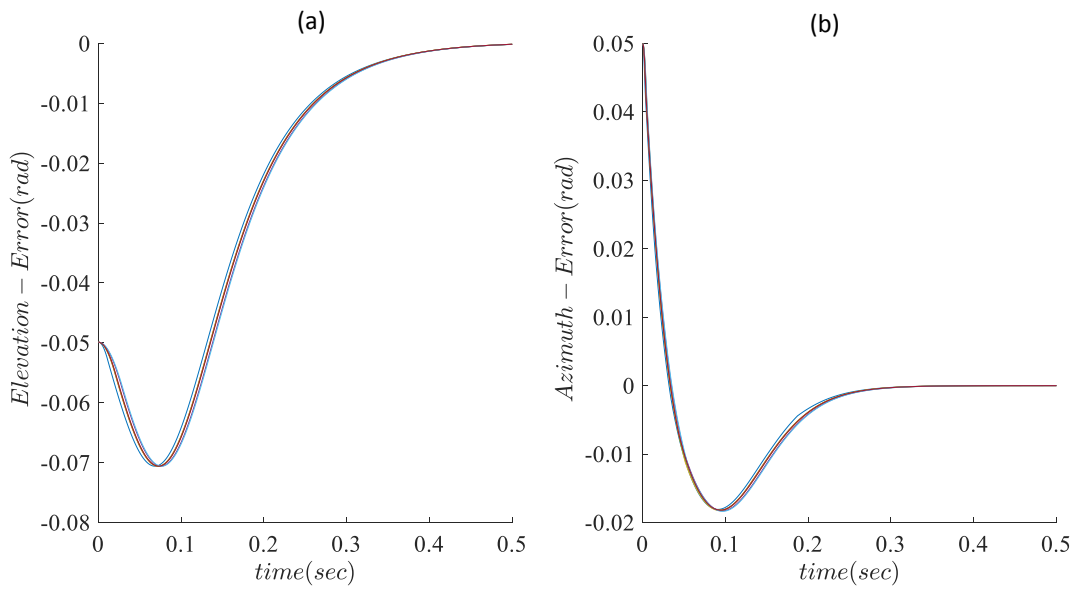


Fig. 12. The angular error of the target and the seeker in the presence of uncertainty

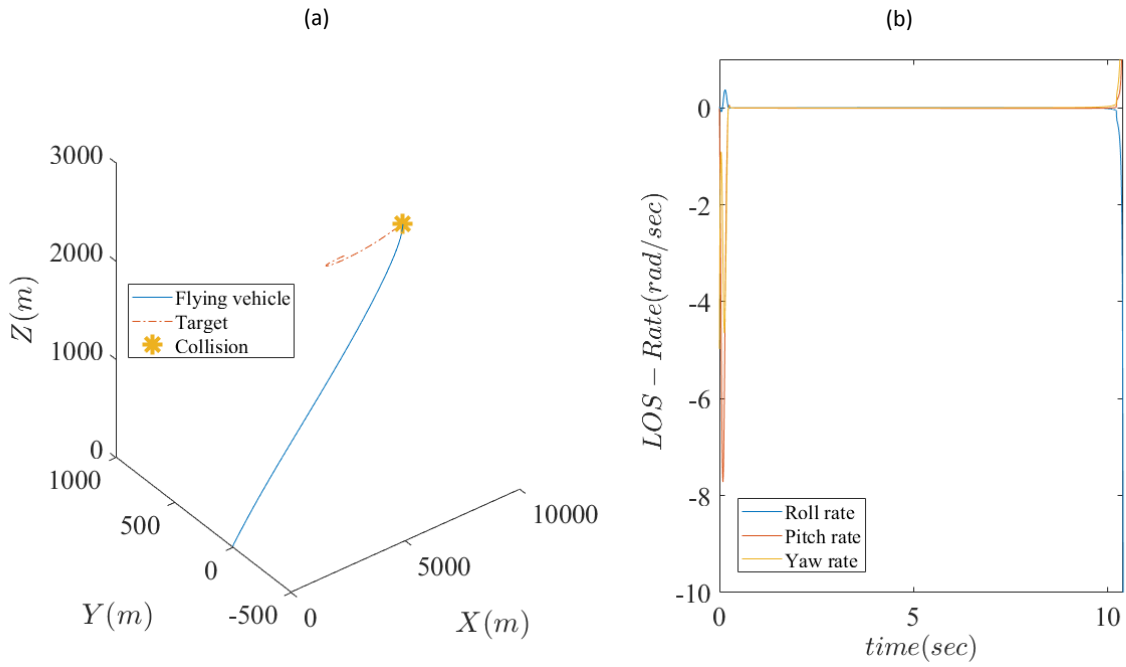


Fig. 13. Line of sight rotation rate and tracking geometry when using a roll-yaw seeker: a) Line of sight rotation rate, b) Target and vehicle trajectory.

attached to the vehicle is simulated in the guidance loop with the PN guidance law. Figure 13 shows the line of sight rotation rate and the trajectory of the target and the vehicle during the simulation. In this simulation, a highly maneuverable target is used in which the acceleration of the target along Y_B axis is $a_y = 3g$ and along Z_B axis is $a_z = 5g$

According to Figure 13, The simulation results demonstrate that the control system can to maintain stability and tracking accuracy even under challenging conditions.

6- Conclusion

This article modeled the dynamics of the two-degree-of-freedom roll-pitch seeker using the Newton-Euler method. The seeker exhibited strong coupling and nonlinear behavior, making it a challenging system to control. To address the singularity problem in this seeker, a method for removing the singularity condition was proposed, and a sliding mode controller was designed for the two-input, two-output system. The simulation results demonstrate that the controller and the method used to eliminate singularity conditions produced a suitable response with zero tracking error. As sliding mode control is known for its robustness, the presence of uncertainty was further simulated to show that the controller is resistant to such conditions.

Nomenclature

- p flying vehicle's roll rate, expressed in the body frame.
- q flying vehicle's pitch rate, expressed in the body frame.
- r flying vehicle's yaw rate, expressed in the body frame.

- p_R roll rate of the outer frame, expressed in the outer frame.
- q_R pitch rate of the outer frame, expressed in the outer frame.
- r_R yaw rate of the outer frame, expressed in the outer frame.
- p_Y roll rate of the inner frame, expressed in the inner frame.
- q_Y pitch rate of the inner frame, expressed in the inner frame.
- r_Y yaw rate of the inner frame, expressed in the inner frame.
- $[\mathbf{I}_R^R]^R$ the moment of inertia matrix of the outer gimbal, expressed in the outer frame.
- $[\mathbf{I}_Y^Y]^Y$ the moment of inertia matrix of the inner gimbal, expressed in the inner frame.
- $u(t)$ control input.
- \mathbf{l} angular momentum.
- φ flying vehicle's roll angle.
- θ flying vehicle's pitch angle.
- ψ flying vehicle's yaw angle.
- φ_s the angle between the body frame and the outer frame.
- ψ_s the angle between the outer frame and the inner frame.
- $\Delta\varphi_s$ the roll error required by the seeker to be positioned

towards the target.

$\Delta\psi_s$ the yaw error required by the seeker to be positioned towards the target.

ω angular velocity vector.

θ_{el} elevation angle.

θ_{az} azimuth angle.

η sliding mode control gain.

λ sliding mode control gain.

ϕ boundary layer thickness.

B Body frame.

I Inertial frame.

Y Inner frame of the seeker.

R Outer frame of the seeker.

B related to the body frame.

I related to the inertial frame.

Y related to the inner frame of the seeker.

R related to the outer frame of the seeker

S related to the seeker.

d desired value.

Appendix: Simulation Parameter Values

In this research, moment of inertia matrix values in the roll-pitch seeker are considered as follows:

$$\begin{aligned} [\mathbf{I}_R^R]^R &= \begin{bmatrix} 0.001 & 0 & 0 \\ 0 & 0.0001 & 0 \\ 0 & 0 & 0.001 \end{bmatrix} \\ [\mathbf{I}_P^P]^P &= \begin{bmatrix} 0.001 & 0 & 0 \\ 0 & 0.0001 & 0 \\ 0 & 0 & 0.001 \end{bmatrix} \end{aligned} \tag{62}$$

To generate the torque, the information of a direct current motor produced by Northrup Grumman Company was used, which is shown in Table 1 [24].

The proportional controller parameters in the tracking loop are listed in Table 2. The parameter k_{p1} is the yaw channel control gain and k_{p2} is the roll channel control gain for the tracking loop proportional controller; The selection criteria of these control gains is to minimize the tracking error.

Also the values of the controller parameters are presented in Table 3.

Table 1. DC motor specifications.

description	Unit	Value	Parameter
Terminal resistance	Ω	4.5	R_a
Terminal inductance	H	0.003	L_a
Torque constant	N.m/A	0.85	K_{TM}
Back EMF	v/Rad/s	0.85	k_e

Table 2. Proportional controller parameters for roll-pitch seeker tracing loop

Value	Parameter
50	k_{p1}
200	k_{p2}

Table 3. Sliding mode controller parameters for the roll-pitch seeker stabilization loop.

description	value	parameter
Pitch channel gain control	200	η_1
The slope of the sliding surface in pitch channel	20000	λ_1
Roll channel control gain	150	η_2
The slope of the sliding surface in roll channel	12000	λ_2
Pitch channel boundary layer thickness	0.4	ϕ_1
Roll channel boundary layer thickness	0.4	ϕ_2
Pitch channel uncertainty upper limit	b_1 0.5	b_1^+
Pitch channel uncertainty lower limit	b_1 -0.5	b_1^-
Roll channel uncertainty upper limit	b_2 0.5	b_2^+
Roll channel uncertainty lower limit	b_2 -0.5	b_2^-

The engine transfer function is as follows:

$$G(s) = 5 \frac{K_{TM}}{(L_a s + R_a) \times (J_m^* s + a_m^*) + K_c K_{TM}} \quad (63)$$

In which $a_m^* = 0$ and $J_m^* = J_m + J_L$. In the block diagram of the tracking and stabilization loops, the DC-motor block means the motor transfer function. Also, in the simulation, the saturation limit of input voltage and output current is considered as $\pm 20V$ and $\pm 2A$ respectively.

References

- [1] Liu, Xiao, and Bo Mo. "Line-of-sight estimation for missile with roll-pitch seeker." 2018 37th Chinese Control Conference (CCC). IEEE, 2018.
- [2] WANG, Zhi-wei, Zai-kang Qi, and Jiang Wang. "Tracking principle for roll-pitch seeker." *Infrared and Laser Engineering* 2 (2008).
- [3] Lin, De-fu, Zhi-wei Wang, and Jiang Wang. "Singularity analysis of roll-pitch seeker and its control strategy." *Transactions of Beijing Institute of Technology* 30.11 (2010): 1265-1269.
- [4] Jiang, Huhai, Hongguang Jia, and Qun Wei. "Analysis of zenith pass problem and tracking strategy design for roll-pitch seeker." *Aerospace Science and Technology* 23.1 (2012): 345-351.
- [5] Liu, Hui, et al. "LOS Stabilization and gyro configuration analysis for roll-pitch seeker." *Applied Mechanics and Materials*. Vol. 397. Trans Tech Publications Ltd, 2013.
- [6] Wu, H., H. Jia, and Q. Wei. "Optimization of angle increments in tracking loop for roll-pitch seekers." *Opt Precis Eng* 22 (2014): 2787-2795.
- [7] Park, Jaemin, et al. "Optimal Control of Roll-Pitch Seeker with Singularity Avoidance." 2018 26th Mediterranean Conference on Control and Automation (MED). IEEE, 2018.
- [8] Wang, Xinchun, et al. "Predictive functional control-based zenith pass controller design for roll-pitch seeker." *International Journal of Aerospace Engineering* 2020 (2020).
- [9] Junlin, M. A., et al. "Design of Micro-miniature Infrared Seeker with Roll-Pitch Structure." 43.5 (2021): 411-416.
- [10] Yue, L. I., H. E. Lei, and X. I. A. Qunli. "Line-of-sight rates extraction of roll-pitch seeker under anti-infrared decoy state." *Journal of Systems Engineering and Electronics* 32.1 (2021): 178-196.
- [11] Jianping, Z. H. O. U., et al. "Stability Design of Spinning Missile Autopilot Considering Parasitical Loop of Roll-pitch Seeker." *Acta Armamentarii* 43.1 (2022):1
- [12] Ghasemi, Mahsa, Hadi Nobahari, and Hamed Mohammadkarimi. "Modeling and Sliding Mode Control of a Roll-Pitch Seeker." *Journal of Aeronautical Engineering* 25.1 (2023): 76-90.
- [13] Chen, Jian, et al. "Snake-hot-eye-assisted multi-process-fusion target tracking based on a roll-pitch semi-strapdown infrared imaging seeker." *Journal of Bionic Engineering* 19.4 (2022): 1124-1139.
- [14] Xiao, Bowen, et al. "Research on the Influence of the Parasitic Loop of the Roll-Pitch Seeker on the Stability of the Guidance System." *Journal of Physics: Conference Series*. Vol. 2508. No. 1. IOP Publishing, 2023.
- [15] Fathi, A., et al. "Modelling and simulation of two axes gimbal fuzzy PI stabilization system in the presence of feedback sensors noise." *IOP Conference Series: Materials Science and Engineering*. Vol. 1172. No. 1. IOP Publishing, 2021.
- [16] Li, Yue, et al. "A new compensation method for DRR of a roll-pitch seeker based on ESO." *International Journal of Aerospace Engineering* 2021 (2021): 1-19.
- [17] Yue, L. I., et al. "Influence of roll-pitch seeker DRR and parasitic loop on Lyapunov stability of guidance system." *Journal of Systems Engineering and Electronics* 32.6 (2021): 1509-1526.
- [18] Lin, Fan, and Xinjie Shen. "Research on Command Generation Strategy of Roll and pitch seeker." *Journal of Physics: Conference Series*. Vol. 2085. No. 1. IOP Publishing, 2021.
- [19] YAO, Jiazhi, et al. "Research on Tracking Strategy of Roll-pitch Seeker." *Acta Armamentarii* (2023): 0.
- [20] Xiao, Bowen, et al. "Research on the Influence of the Disturbance Rejection Rate of a Roll-Pitch Seeker on Stable Tracking Characteristics." *Aerospace* 10.11 (2023): 940.
- [21] Xiao, Bowen, et al. "Research on the Influence of the Parasitic Loop of the Roll-Pitch Seeker on the Stability of the Guidance System." *Journal of Physics: Conference Series*. Vol. 2508. No. 1. IOP Publishing, 2023.
- [22] JIN, Qiuyan, et al. "The Control Strategy of Zenith-pass Singularity Problem Under the Roll-pitch Seeker Oblique Scheme." *Acta Armamentarii* 45.2 (2024): 628.
- [23] Zipfel, P. H. "Modeling and Simulation of Aerospace Vehicle Dynamics—Third edition." (2014).
- [24] Abdo, Maher Mahmoud, et al. "Stabilization loop of a two axes gimbal system using self-tuning PID type fuzzy controller." *ISA transactions* 53.2 (2014): 591-602.
- [25] Slotine, Jean-Jacques E., and Weiping Li. *Applied nonlinear control*. Vol. 199. No. 1. Englewood Cliffs, NJ: Prentice hall, 1991.

HOW TO CITE THIS ARTICLE

M. Ghasemi, H. Nobahari, H. Mohammadkarimi, *Modeling and Integral Sliding Mode Control of a Roll-yaw Seeker by Removing the Singularity Condition*, *AUT J. Model. Simul.*, 56(2) (2024) 235-256.

DOI: [10.22060/miscj.2025.23515.5380](https://doi.org/10.22060/miscj.2025.23515.5380)



